

Flaw effects on square and kagome artificial spin ice

M. Di Pietro Martínez^{*1,2} and R. C. Buceta^{†1,2}

¹Instituto de Investigaciones Físicas de Mar del Plata, UNMdP and CONICET

²Departamento de Física, FCEyN, Universidad Nacional de Mar del Plata
Funes 3350, B7602AYL Mar del Plata, Argentina

October 19, 2016

Abstract

In this work, we study the effect of nanoislands with design flaws on the bilayer-square and in kagome arrays of artificial spin ice. We have introduced disorder as random fluctuations in the length of the magnetic islands using two kinds of distributions: Gaussian and uniform. For artificial square ice, as the system behaviour depends on its geometrical parameters, we focus on studying the system in the proximity of the Ice-like configuration where nearest neighbour and next nearest neighbour interactions between islands are approximately equal. We show how length fluctuations of nanoislands affect the antiferromagnetic and (locally) ferromagnetic ordering, by inducing the system, in the case of weak disorder, to return to the Ice-like configuration where antiferro- and ferromagnetic vertices are equally likely. Moreover, in the case of strong disorder, ferromagnetic vertices prevail regardless of whether the mean length corresponds or not to an antiferromagnetic ordering. Additionally, for strong disorder we have found that excitations are not completely vanished in the ground state. We also study kagome arrays inducing a similar crossover between types of vertex and show how disorder can lead to a steady mixed-state where both types of monopoles are present.

Keywords: Frustration, geometry, dipolar interaction, disorder, spin ice, degrees of freedom.

1 Introduction

Artificial spin ices are counterparts to natural spin ice materials such as rare earth pyrochlores [1]. Both are magnetic systems with frustrated interactions that show unusual collective behaviours and distinctive complex patterns [2, 3]. Magnetic ions in pyrochlore compounds are located in the corners of tetrahedra and the local interaction energy is minimized when the moments order according to Pauling's ice rule: two spins pointing inwards and two outwards of each tetrahedron [4]. This rule was originally proposed for the proton orderings in (cubic) water ice but a perfect mapping with spin ice materials such as the one mentioned above was found later (see Figure 1 (a) and (b)). Geometric frustration of pyrochlore materials enables highly degenerate ground states of the spin ice manifested as a large residual entropy even at very low temperatures [5]. Artificial spin ice (ASI) consists of a lithographically manufactured two-dimensional array of ferromagnetic nanoislands with a strong shape anisotropy resulting in single-domains that behave like giant Ising

^{*}mdpietro@ifimar-conicet.gob.ar

[†]rbuceta@mdp.edu.ar

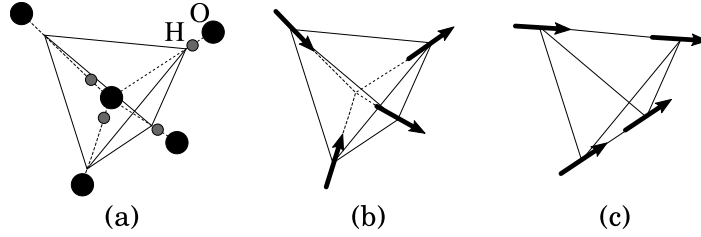


Figure 1: (a) Hydrogen and Oxygen atoms' position in water ice. (b) Magnetic moments in spin ice compounds, such as $\text{Ho}_2\text{Ti}_2\text{O}_7$ [1]. (c) Magnetic moments in a bilayer artificial spin ice.

spins. Magnetic force microscope images show that the magnetic moment of each island is indeed aligned along its long axis [6], which confirms the dominance of shape anisotropy over the low magnetocrystalline anisotropy of Permalloy, one of the materials used in the manufacture of ASI. The appropriate choice of material, geometry and array topology leads to different characteristic collective behaviors.

The islands of the square ASI are placed in the links of a square lattice, as we show in Figure 2 (a). The four spins set around a given vertex have 16 possible configurations, classified into four topological types T_n , with $n = 1, \dots, 4$ (see Figure 2 (b)). Note that T_1 and T_2 satisfy the ice rules meeting $\nabla \cdot \mathbf{S} = 0$, while T_3 and T_4 do not. If the dipoles are oriented randomly and not interacting, $3/8$ of the vertex population corresponds to T_1 and T_2 . Wang *et al.* [6] observed that, in lattices with fixed island size, this holds for large lattice spacing, while for smaller lattice spacing T_1 and T_2 population increases approximately to $7/10$, which shows the preponderance of the Ice-type spin configuration. The easiest way to create an excitation is to flip a single spin turning a T_1 or T_2 vertex into T_3 . By doing this, sources or defects are being created, making the flow nonzero, or locally $\nabla \cdot \mathbf{S} = \pm 2$. Thus, the magnetic defects interact as Coulombian charges, which are called monopoles [7, 8]. However, in two-dimensional square ASI, monopoles do not appear as effective low-energy configurations, as they do in three-dimensional materials [9]. When the ice rule is not met, a monopole-antimonopole pair that is not fixed is created, even though they are able to move separately by flipping spins, until the called ‘Dirac-string’ between defects bumps into another defect or the loop is closed. The creation of this pair of mobile defects is known as fractionalization of the excitation [10]. The square-ice model (or six-vertex model [11]) fulfills the condition $J_1 = J_2$ where J_1 and J_2 are the nearest-neighbour and next-nearest-neighbour energy, respectively, as we show in Figure 2 (a). Then, the energies of vertices T_1 and T_2 (namely E_1 and E_2 respectively) are degenerate and the system orders according only to Ice-like configurations. In the case of inequality the F-model is obtained instead, which consists of spin configurations T_1 and T_2 , with $E_2 > E_1$. In square ASI, at low temperatures, the configurations of the F-model are expected. The inequivalence in the properties of the vertices T_1 and T_2 on square ASI causes it to be weakly frustrated, like the F-model, when $J_1 \neq J_2$ [12]. In contrast, in the three-dimensional spin ice interactions between pairs of spins in a vertex are equivalent. In square ASI this can also be achieved by slightly changing the geometry of the array.

In order to recover the equivalence on vertex interactions, Möller and Moessner [13] proposed a bilayer square ASI, made of two sublattices spaced a distance h , each of which is composed by unidirectional magnetic islands, designed such that when $h = 0$ the two-dimensional square ASI with its properties is recovered. By adjusting the gap distance h , it is possible to establish degenerate states of energy for all those vertices which obey the ice rule; the centers of the islands form a tetrahedron (see Figure 1 (c)) and the ordering disappears, allowing monopoles to move freely. For this system, the authors showed [14] that the monopoles are excitations that have two types of Coulombian interactions: one three-dimensional magnetic and another two-dimensional entropic with logarithmic behaviour. Considering point-like dipoles for the degenerate state (taking $J_1 = J_2$) they obtained [13] that the gap parameter is $h_{\text{ice}} \approx 0.419 a$, where a is the lattice spacing. In contrast to elongated dipoles, as it increases its length d the ice gap parameter decreases

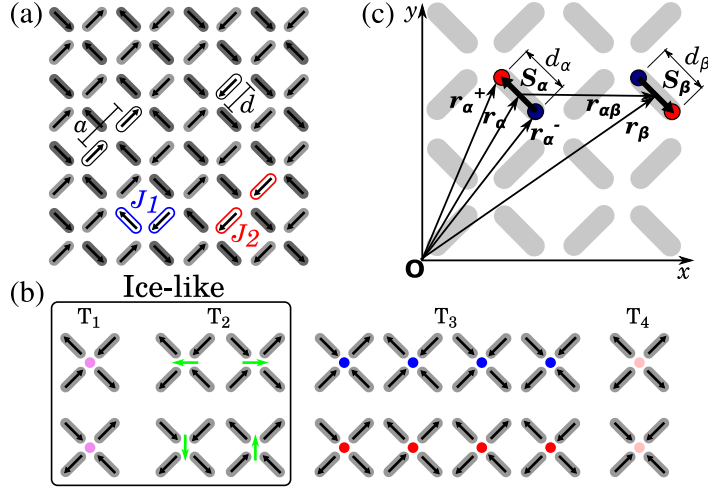


Figure 2: (a) Square spin ice array simulated in this work: a is the lattice parameter, d is the island length and J_1 and J_2 are the nearest and the next nearest neighbour energy, respectively. There is also a gap distance h between dipoles pointing in different directions which are shown in the figure with different shades of gray. (b) There are 16 possible moment configurations for the four islands' vertex. Furthermore, these can be classified into four different topological groups T_n , with $n = 1, \dots, 4$. T_1 and T_2 satisfy the ice rules while the other two do not. (c) Coordinate system used in our calculations. This illustrative figure only shows two dipoles \mathbf{S}_α and \mathbf{S}_β of the same layer. Each dipole-like spin \mathbf{S}_κ is considered a needle, with its center located at \mathbf{r}_κ , formed by two opposite charges $\pm q$ placed at \mathbf{r}_κ^\pm ($\kappa = \alpha, \beta$). Additionally, $\mathbf{r}_{\alpha\beta} = \mathbf{r}_\beta - \mathbf{r}_\alpha$ is the spin relative position of \mathbf{S}_β respect to \mathbf{S}_α .

(particularly when $d = a$ we have $h_{\text{ice}} = 0$). Shortly afterward, Mol *et al.* [15] studied the ground states and excitations as a function of h . They showed that there is anisotropy in the tension of the ‘Dirac-string’ and that the quantity of magnetic charge is dependent on the direction of the monopoles’ movement, showing an abrupt change when monopoles are separated along the major axis of the islands. Additionally, for point-like dipoles, these authors found that the ground state changes for $h'_{\text{ice}} \approx 0.444a$, attributing this slight deviation to one of the configurations with ice rule which has no ground state energy, *i.e.* the system is not in a completely degenerate state.

Since the pioneering work of Wang *et al.* [6] on square ASI [16, 17], other two-dimensional lattices with regular geometries have been studied, such as triangular [14, 15, 17–22], honeycomb or kagome [23–25], brick-work [26] and pentagonal or shakti [27, 28]. Particularly, square and kagome ASI complement each other. The kagome ASI consists on an array of islands on the links of a honeycomb lattice. While square ASI has an even coordination number, kagome ASI has an odd coordination number, which implies that its 2^3 possible vertices are all monopole like. Also, as the interaction between each pair of islands set around a given vertex is equivalent, there is no need for a gap distance like in square ice.

In this paper, we have studied the influence of design flaws of the nanoislands on the thermodynamic properties and dynamics of the system, for a bilayer-square and kagome ASI. Here, we have considered random fluctuations in the length d of the magnetic islands for two prototypical cases: Gaussian and uniform distributions. In the square ASI case, we have focused on studying the system at points of the parameter space (d, h) in a neighbourhood of the point $(d, h_{\text{ice}}(d))$ where the condition $J_1 = J_2$ is met. We show how length fluctuations of nanoislands affect the antiferromagnetic and ferromagnetic ordering, *i.e.* $J_2 \lesssim J_1$ and $J_2 \gtrsim J_1$, respectively, at low temperatures where populations of vertices T_1 and T_2 prevail. Similarly, we have studied the effects of designs flaws over kagome ASI. In Section 2 we give theoretical background of the needle model and our simulation details. In Section 3, we show the results achieved for the vertex population, the specific heat, the acceptance as a function of temperature and we also provide a comprehensive study

for the observed effects. Finally, in the Conclusions section, we evaluate the outcomes obtained, showing the importance of the presence of the design flaws in the thermodynamic properties of the vertices that satisfy the ice rule.

2 The needles model

We have considered the island moments (or spins) $\mathbf{S}_\kappa = \mu \hat{S}_\kappa$ as breadthless needles of finite length, each of which is a dipole formed by two effective charges $\pm q_\kappa = \mu/d_\kappa$ located at \mathbf{r}_κ^\pm and separated by a distance d_κ (see Figure 2 (c)). Thus, the potential created by a needle-dipole at a point \mathbf{r} is simply

$$\Phi_\kappa(\mathbf{r}) = \frac{q_\kappa}{4\pi\epsilon_0} \left(\frac{1}{|\mathbf{r} - \mathbf{r}_\kappa^+|} - \frac{1}{|\mathbf{r} - \mathbf{r}_\kappa^-|} \right), \quad (1)$$

and the interaction energy between two dipole-like spins \mathbf{S}_α and \mathbf{S}_β is

$$\mathcal{U}_{\alpha\beta} = q_\beta [\Phi_\alpha(\mathbf{r}_\beta^+) - \Phi_\alpha(\mathbf{r}_\beta^-)].$$

Taking into account that $\mathbf{r}_\kappa^\pm = \mathbf{r}_\kappa \pm \frac{1}{2} d_\kappa \hat{S}_\kappa$ (with $\kappa = \alpha, \beta$) and $\mathbf{r}_{\alpha\beta} = \mathbf{r}_\beta - \mathbf{r}_\alpha$, the equation above can be rewritten as

$$\mathcal{U}_{\alpha\beta} = \frac{\mathcal{D}}{d_\alpha d_\beta} \left(\frac{1}{|\mathbf{r}_{\alpha\beta} + \frac{1}{2}(d_\beta \hat{S}_\beta - d_\alpha \hat{S}_\alpha)|} + \frac{1}{|\mathbf{r}_{\alpha\beta} - \frac{1}{2}(d_\beta \hat{S}_\beta - d_\alpha \hat{S}_\alpha)|} - \frac{1}{|\mathbf{r}_{\alpha\beta} + \frac{1}{2}(d_\beta \hat{S}_\beta + d_\alpha \hat{S}_\alpha)|} - \frac{1}{|\mathbf{r}_{\alpha\beta} - \frac{1}{2}(d_\beta \hat{S}_\beta + d_\alpha \hat{S}_\alpha)|} \right). \quad (2)$$

where $\mathcal{D} = \mu_0 \mu^2 / 4\pi$. As can be proved, the expression for $\mathcal{U}_{\alpha\beta}$ corresponds to the dipolar energy when $d_\kappa \rightarrow 0$ ($\kappa = \alpha, \beta$). Note that, since $\mathbf{r}_{\alpha\beta} = \mathbf{r}_{\alpha\beta}(a, h)$, the interaction energy depends on the fixed geometric parameters a , h and d_κ of the lattice, and so does the system's behaviour. Remembering that in the case of kagome ASI $h = 0$. We have assumed that the length of the nanoislands is $d_\kappa = d + \eta_\kappa$, where η_κ is the length fluctuation with mean value $\langle \eta_\kappa \rangle = 0$ and correlations $\langle \eta_\alpha \eta_\beta \rangle = C_{\alpha\beta}$. If the length fluctuations are independent random variables the cross-correlation is zero and $C_{\alpha\beta} = C \delta_{\alpha\beta}$.

Taking into account that $\mathcal{U}_{\alpha\beta} = \mathcal{U}_{\beta\alpha}$, the system total energy $E = \frac{1}{2} \sum_{\alpha\beta} \mathcal{U}_{\alpha\beta}$ can be expressed as

$$E = \frac{1}{2} \sum_{\alpha \neq f} \sum_{\beta \neq f} \mathcal{U}_{\alpha\beta} + \sum_{\alpha \neq f} \mathcal{U}_{\alpha f}, \quad (3)$$

where f is the index of the spin to flip and wherein self-interactions are excluded, *i.e.* $\alpha \neq \beta$. The interaction energy after the spin \mathbf{S}_f is flipped verifies

$$\mathcal{U}'_{\alpha\beta} = \begin{cases} \mathcal{U}_{\alpha\beta} & \text{if } \alpha \neq f \text{ and } \beta \neq f \\ -\mathcal{U}_{\alpha\beta} & \text{if } \alpha \neq f \text{ and } \beta = f, \end{cases} \quad (4)$$

Therefore, the change of the system's total energy $\Delta E_f = E' - E$, where E' is the total energy with \mathbf{S}_f flipped, becomes

$$\Delta E_f = -2 \sum_{\alpha \neq f} \mathcal{U}_{\alpha f}. \quad (5)$$

For square ice, in order to find the point $(d, h_{\text{ice}}(d))$ where the condition $J_1 = J_2$ is met, we have calculated the interaction energy between a pair of dipoles in a vertex. The energy $J_1^{\{\alpha, \beta\}}$ due to the interaction between nearest-neighbour dipoles $\{\alpha, \beta\}$ is obtained taking $\mathbf{r}_{\alpha\beta} = (\frac{a}{2}, \frac{a}{2}, h)$, $\mathbf{S}_\alpha = (0, 1, 0)$ and $\mathbf{S}_\beta = (1, 0, 0)$ in Equation 2. Likewise, the energy $J_2^{\{\alpha, \beta\}}$ due to the interaction

between next-nearest-neighbour dipoles $\{\alpha, \beta\}$ is obtained taking $\mathbf{r}_{\alpha\beta} = (0, a, 0)$ and $\mathbf{S}_\alpha = \mathbf{S}_\beta = (0, 1, 0)$ in Equation 2. In our model, as the lengths are considered to fluctuate between islands, the vertex energies $J_n^{\{\alpha, \beta\}}$ ($n = 1, 2$) are also different, and the ice rule is a local property that is approximately fulfilled. To order zero in the length fluctuations, *i.e.* $J_n = J_n^{\{\alpha, \beta\}}|_{\eta_\alpha=\eta_\beta=0}$, the condition $J_1 = J_2$ is fulfilled over the entire lattice.

We have performed Monte Carlo simulations with the Metropolis algorithm using Equations 2 and 5 over a square ASI of size $N = 900$ spins, with periodic boundary conditions and a cut-off of $14a$ for the dipolar sum, and over a kagome ASI of $N = 675$ spins, with a cut-off of $15a$. In order to avoid the characteristic low-temperature freezing we also used the loop-move method [29, 30].

3 Results

3.1 Fluctuations in Square Ice

Having studied a system consisting of nanoislands with equal length and obtained a behaviour that is in agreement with previous results [14, 31], let us examine now what happens if they do not have the same length. Each flawed island is fixed with a length $d_\kappa = d + \eta_\kappa$, where the length fluctuation η_κ is a random number chosen according to the probability density $P(\eta_\kappa)$ and the constant d is the mean length. For weak disorder, $P(\eta_\kappa)$ is a Gaussian with standard deviation σ and zero mean; while for strong disorder we use a uniform distribution as to avoid $d_\kappa > a$. Then η_κ is uniformly selected from the interval $(-\Delta, \Delta)$. In Figure 3, we show the effect of different intensity of disorder.

We have studied the system by choosing the mean length $d = \langle d_\kappa \rangle$ and the gap distance h between sublattices such that $J_1 = J_2$ is verified. In order to study what happens nearby this condition, the geometrical parameters were set at $h = 0.205a$ and $d_- = 0.702a$ or $d_+ = 0.704a$. In the absence of flaws, the former mean length brings the antiferromagnetic ground state with prevalence of vertices T_1 . In contrast, also in absence of flaws, the latter mean length corresponds to a (locally) ferromagnetic ground state with predominance of vertices T_2 . In Figure 3, where plots (a) and (c) correspond to the vertex population for each configuration type and plots (b) and (d) are the corresponding specific heat, we show the simulation results of the system of nanoislands with the same mean length and several intensity of length fluctuations with Gaussian and uniform distributions. Vertex population plots show that, independently of the design flaws, the high temperature equilibrium state corresponds to a random state where each vertex type has a population related to the number of possible configurations, *i.e.* T_1 : 1/8, T_2 : 1/4, T_3 : 1/2 and T_4 : 1/8 (see Figure 2 (b)). Also, both plots show how the adimensionalized temperature $t = a^3 k_B T / \mathcal{D}$ exhibits a transition at $t = t_1^* \approx 4$ which is not affected by existing flaws in the system. Below this transition ($t < t_1^*$) the population of vertices T_3 , which corresponds to excitations, falls until it vanishes completely. The plots of specific heat display a peak for this first transition, which confirms that the system behaviour is not affected by the flaws. In systems without length flaws or with weak length fluctuations, at lower temperatures, a second peak appears at $t = t_2^* \approx 0.2$ in the specific heat. This peak reveals a second transition whose behaviour is known in systems without flaws, which accounts for meaningful variations in populations of vertices T_1 and T_2 . For systems without flaws, below this second transition ($t < t_2^*$) the population of vertices T_2 or T_1 increase to 100% when the temperature decreases (see Figure 3 (a) and (c), respectively). When $d = d_-$ (see Figure 3 (a)) a crossover of T_1 - T_2 populations is observed at $t = t_2^*$. For $\sigma = 0.01$, we have found that even though the T_1 - T_2 crossover has not disappeared, in the ground state T_1 population has increased at the expense of T_2 population and the specific heat maximum has been significantly reduced. Similarly in Figure 3 (c), T_2 population has increased at the expense of T_1 population. Then, we have established that in the case of weak fluctuations, which correspond to $\sigma \lesssim 0.05$, while $t < t_2^*$ the T_1 and T_2 populations start to redistribute until the Ice-like configuration is

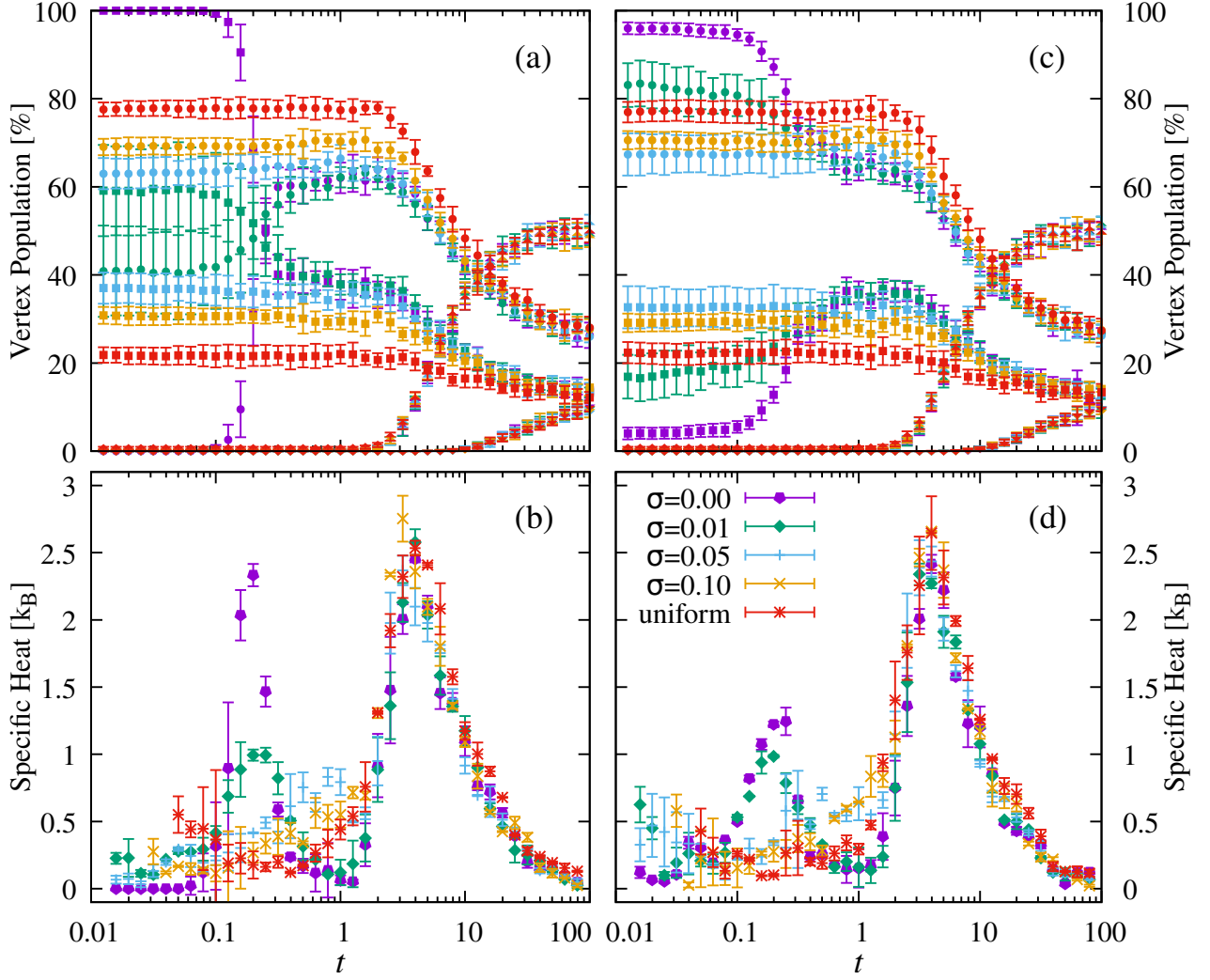


Figure 3: Top: Vertex population *vs.* adimensionalized temperature $t = a^3 k_B T / \mathcal{D}$ for $h = 0.205a$ and (a) $d_- = 0.702a$ or (c) $d_+ = 0.704a$, where T_1 : circles (\bullet), T_2 : squares (\blacksquare), T_3 : up-triangles (\blacktriangle) and T_4 : down-triangles (\blacktriangledown). Bottom: Its corresponding specific heat curves (b) and (d) respectively, for different intensity of length fluctuations, as indicated. The uniform length fluctuation was set using $\Delta = 0.298$ and $\Delta = 0.296$, respectively.

restored. That is to say, T_1 and T_2 vertices are equally likely, and so 1/3 of the vertex population is T_1 and 2/3 is T_2 (see Figure 2 (b)). Furthermore, the second peak of the specific heat flattens.

However, by continuing to increase σ a different behaviour appears. Regardless of whether the system is set as ferro- or antiferro-magnetic, in the ground state T_2 vertices prevail with a population bigger than 2/3. Moreover, in the case of uniformly distributed fluctuations, T_2 population reaches $77 \pm 2\%$, while T_1 population stays at $22 \pm 2\%$. However, this system's behaviour corresponds neither to the random configuration nor to the Ice-like configuration. So, what leads to this effect? Why does strong disorder encourage the prevalence of T_2 vertices? These questions have led us to study if there is a relation between the type of vertex and the length of the islands set around such vertex and how strongly related they are as a function of the temperature and the fluctuation intensity. Thus, we have defined the quantity $f(n, v)$ as the fraction of T_n vertices that have v of the four islands in favour ($v = 0, \dots, 4$). That is to say, T_1 vertices are favoured by islands with a length smaller than the mean value d , while T_2 vertices are the ground state for a system with length greater than d . So, for example, $f(1, 0)$ corresponds to the fraction of T_1 vertices that have none of the four vertices with a length smaller than d . By definition,

$f(n, v)$ meets $\sum_v f(n, v) = 1$. In Figure 4, we show the results achieved for different $\sigma > 0$. High temperature behaviour corresponds to a random disposition of the vertices; therefore the fractions are given by the number of possible configurations: $f(n, 0) = 1/16$, $f(n, 1) = 1/4$, $f(n, 2) = 3/8$, $f(n, 3) = 1/4$ and $f(n, 4) = 1/16$. However, as the temperature is lowered the behaviour changes. For $\sigma = 0.01$, the fraction $f(n, 0)$ decreases to zero as none of the islands favours T_n vertices. In addition, $f(n, 1)$ decreases while $f(n, 2)$ remains constant. In contrast, if $v = 3$ or $v = 4$ the fraction of vertices rises. For this intensity of length fluctuation the results are the same for both T_1 and T_2 , but for $\sigma \geq 0.05$ the curves split into two different branches according to the type of vertex, showing an incipient asymmetry in the nature of the system. Also, the spacing between branches broadens by increasing the fluctuation intensity. While T_1 vertices appear more likely if $v > 2$, T_2 vertices are more permissive and also appear for $v = 2$. Even when there is only one island in favour, a bigger fraction of T_2 vertices accept this situation than T_1 vertices. Considering these results, we can say that a strong spacial relation stressed by fluctuation exists, where T_1 and T_2 vertices are going to be arranged strongly induced by local interaction with islands around the vertex in question. On one hand, weak disorder has a global effect as the system displays a mean field behaviour, which is the reason why the Ice-like configuration is the ground state. On the other hand, strong fluctuations make the vertex type to be a direct result of the short range interactions as a local effect.

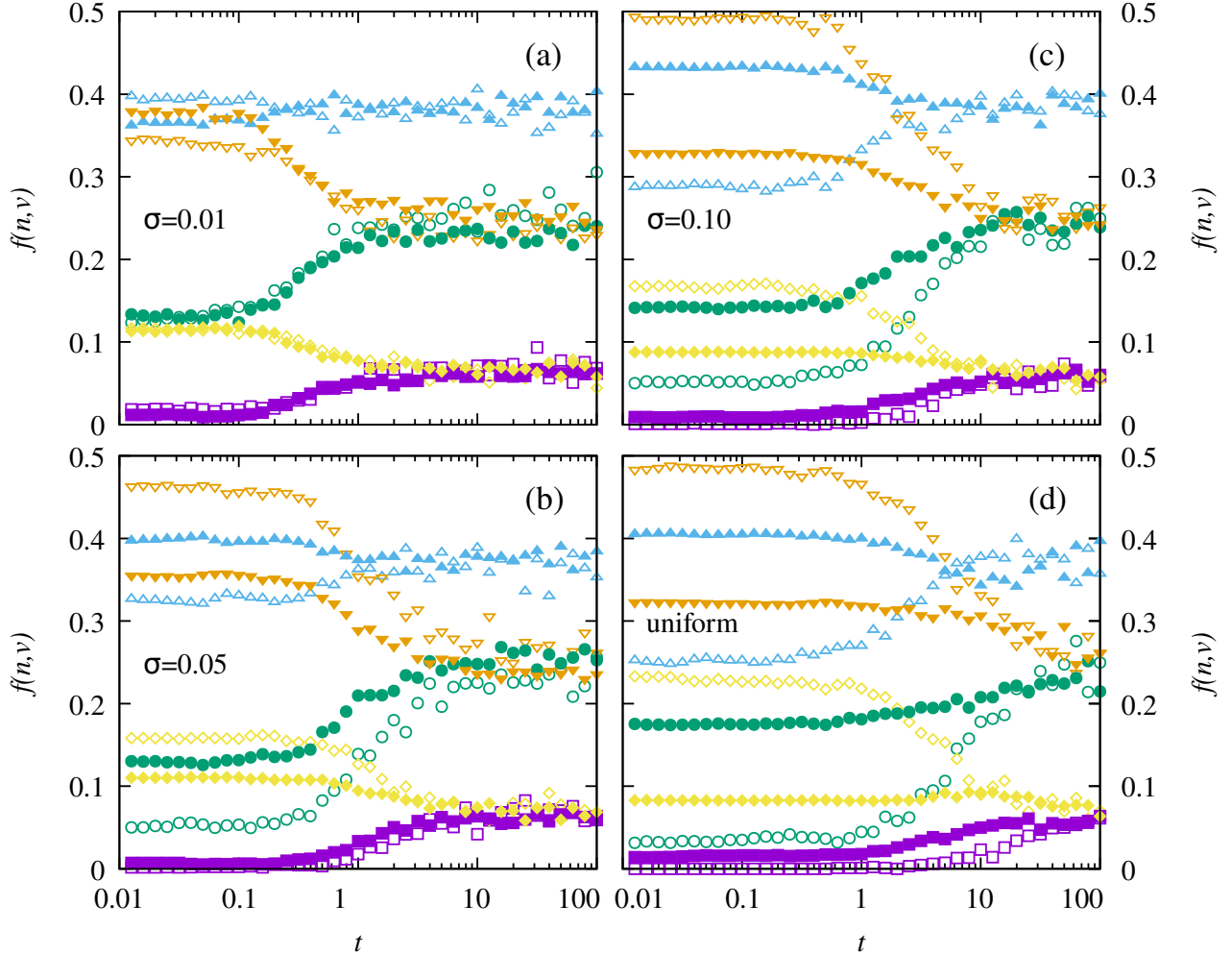


Figure 4: Vertex fraction $f(n, v)$ vs. adimensionalized temperature for different intensity of length fluctuation σ , where $v = 0$: squares (■), $v = 1$: circles (●), $v = 2$: up-triangles (▲), $v = 3$: down-triangles (▼) and $v = 4$: diamonds (◆), and void points correspond to the fraction of T_1 vertices while filled points correspond to the fraction of T_2 vertices.

However, where does this asymmetry come from? We compare now the energies E_1 and E_2 contained in a T_1 or a T_2 vertex, respectively. Figure 5 (b) shows these energies for a vertex surrounded by four islands of the same length d . As discussed previously, when d is smaller than the E_1 - E_2 crossover length d^* the ground state corresponds to the antiferromagnetic state, and when d is greater it corresponds to the ferromagnetic state. However, if one of the four islands has a different length, the energy contained in the vertex changes. In Figure 5 (a) one of the islands has a length $d_4 = 0.9$, and as a result d^* moves leftwards widening the ferromagnetic zone. This implies that the other three islands should be even smaller than they would be in the (b) case to maintain a T_1 vertex. Similarly, in Figure 5 (c), one of the lengths is fixed in $d_4 = 0.5$ and d^* moves rightwards widening the antiferromagnetic zone. However, for a given fluctuation intensity the crossover behaviour is asymmetric and the greater the intensity is, the more evident this effect becomes. Thus, the energy of the system allows the prevalence of T_2 vertices in the ground state when strong flaws are introduced which, combined with the strong spacial relation that reduces the interaction to short-range, results in the observed effect.

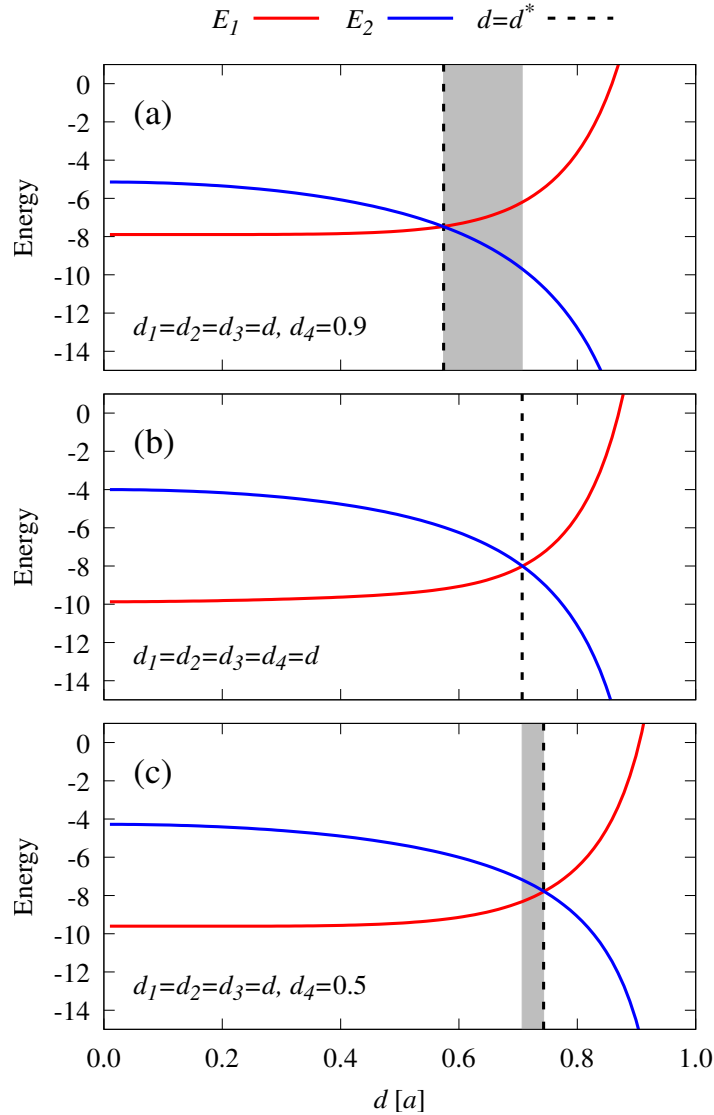


Figure 5: Energy E_n contained in a T_n vertex surrounded by four islands as a function of the island length d . In figure (b) the four lengths are equal, and in figures (a) and (c) one of the islands is fixed at a given value. Dashed lines correspond to E_1 - E_2 crossover and gray areas highlight the difference introduced by fixing one island's length.

Additionally, we have also found a remaining presence of T_3 vertices at any temperature. While for $\sigma < 0.05$, at low temperature the population T_3 sticks at $0 \pm 0\%$, for $\sigma = 0.1$ we have found a population T_3 of $0.3 \pm 0.2\%$. For the uniform distribution, a $0.7 \pm 0.3\%$ of excitations driven by strong fluctuations persist even in the ground state. In order to determine whether this effect is a system freezing issue or not, we studied the ratio of acceptance of spin-flips and loop-moves. In Figure 6, we show the acceptance for different fluctuation intensities. The swapping of vertices T_1 and T_2 introduces an intermediate step with vertex T_3 , *i.e.* the creation of an excitation. Thus, the spin-flip method freezes at $t \approx t_1^*$. The loop-moves are not accepted at first as the population of T_3 vertices is still too big. Then, the loop-moves develop until the ground state is reached and there is no need to continue changing the vertex type. While the curves for spin-flips are not significantly affected by the fluctuation intensity, the curve of loop-move flattens and moves rightward as intensity increases. For low temperature, the population T_3 is about 0.7% in the uniform fluctuation case, an amount too small to justify the 40% to 0.1% reduction of the loop-move acceptance. We also show the acceptance rate using a uniform distribution of fluctuations after a different amount of loop-move steps. Note that the curves are stable even if an order of magnitude in steps is increased. Then, the observed behaviour can be found in the physics of the simulated system.

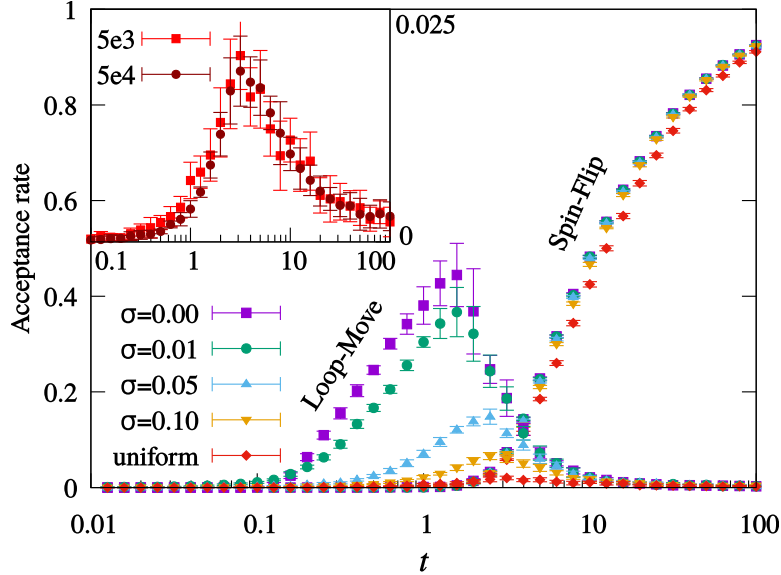


Figure 6: Acceptance rate of spin-flips and loop-moves for different intensity of disorder, as indicated, using $h = 0.205$ and $d_- = 0.702$. The uniform disorder was set using $\Delta = 0.298$. Inset: Acceptance rate using a uniformly distributed fluctuation after a different amount of Loop-Move steps.

3.2 Fluctuations in Kagome Ice

Similarly, in kagome ice we have studied the thermal behaviour of the vertex population for different length-fluctuation intensity. In this case, $J_1 = J_2 = J$ as the distance between each possible pair of islands set around a given vertex is the same. Thus, there is no need to include the gap distance h . Nevertheless, by studying the energy of this system, it can be observed that depending on the values of J and d the system presents two different ground states. A three legged vertex can have 2^3 different configurations, which in turn can be topologically separated in two types of vertices depending on the net charge q . Namely, T_1 are the vertices with $|q| = 1$ while T_3 are the ones with $|q| = 3$. Due to the odd coordination number, unlike the square ice this kind of system has always monopoles present. For $J = 0$ it has been demonstrated in previous studies [14]

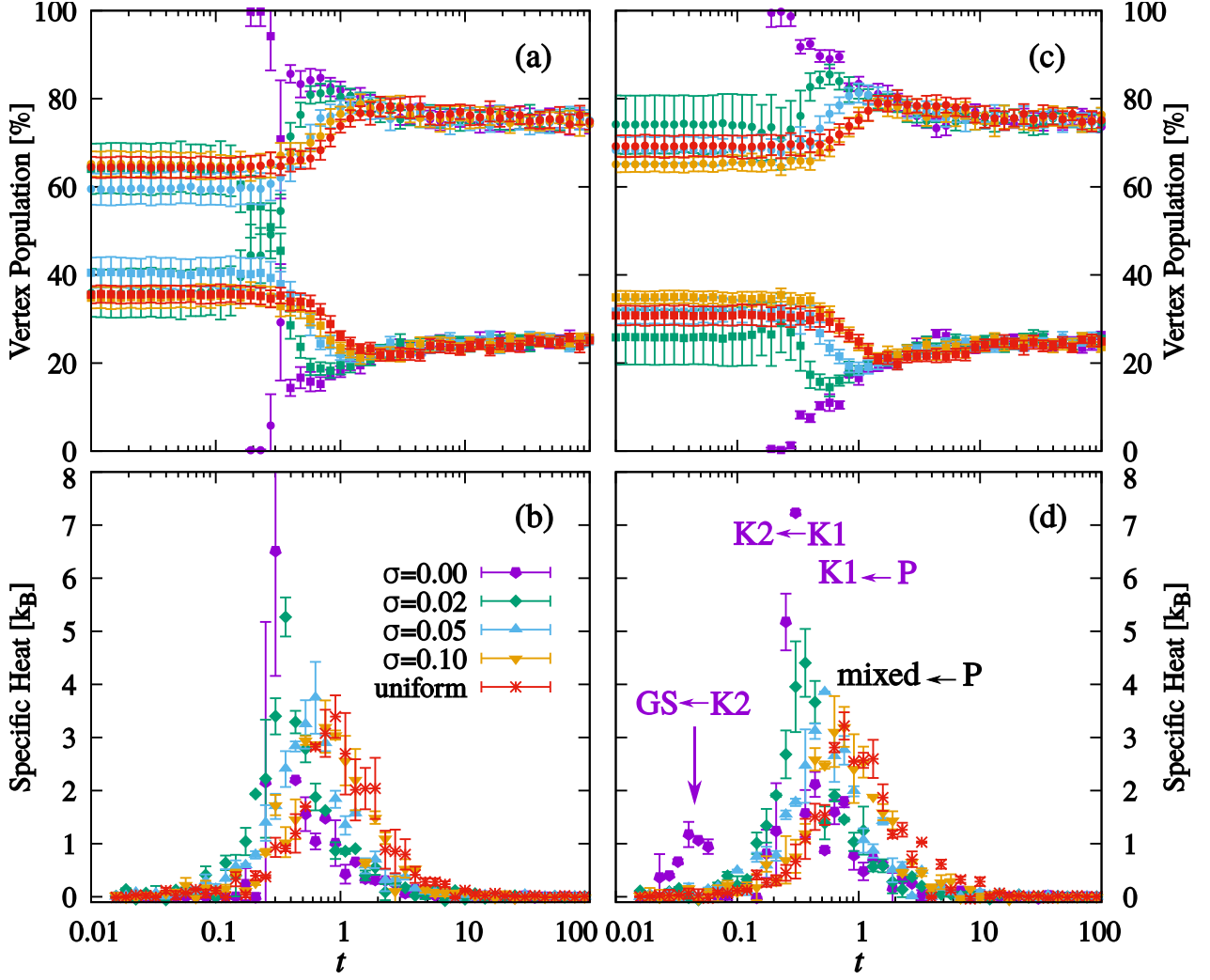


Figure 7: Top: Vertex population *vs.* adimensionalized temperature $t = a^3 k_B T / \mathcal{D}$ for $J = -6\mathcal{D}$ and (a) $d_- = 0.792a$ or (c) $d_+ = 0.794a$, where T_1 : circles (\bullet) and T_3 : squares (\blacksquare). Bottom: Its corresponding specific heat curves (b) and (d) respectively, for different intensity of length fluctuations, as indicated. The uniform length fluctuation was set using $\Delta = 0.208$ and $\Delta = 0.206$, respectively.

that the system passes through four different phases as the temperature is lowered. First, a high temperature behaviour that corresponds to a paramagnetic phase (P) where both T_1 and T_3 vertices are present with probability $3/4$ and $1/4$, respectively. Then, there is a first transition into a T_1 gas called K1, where $q = \pm 1$. Later on, the system rearranges into a charge-ordered phase K2, where $q = +1$ and $q = -1$ vertices are positioned as a NaCl structure. Finally, the system transitions into the final ordered state where T_1 vertices organize also magnetically. Also, a model of “dumbbells” [22], which means $d = 0$, was studied for $J > 0$ and $J < 0$, where the authors show how varying J affects the three peaks corresponding to the transitions described above.

Here, we have extended these results to the complete parameter space (J, d) and we have used it as a tool to induce a similar situation to the one studied for square ice. Thus, we have fixed the parameters $J = -6\mathcal{D}$ and $d_- = 0.792a$ or $d_+ = 0.794a$, as to obtain a condition close to $E_1 = E_3$. In Figure 7 (a) and (c) we show the thermal behaviour of the vertex population for $d = d_{\pm}$ which corresponds to $E_3 \gtrless E_1$, respectively. In any case, high temperature leads to the paramagnetic (P) state. By decreasing the temperature, the first transition into T_1 gas takes place;

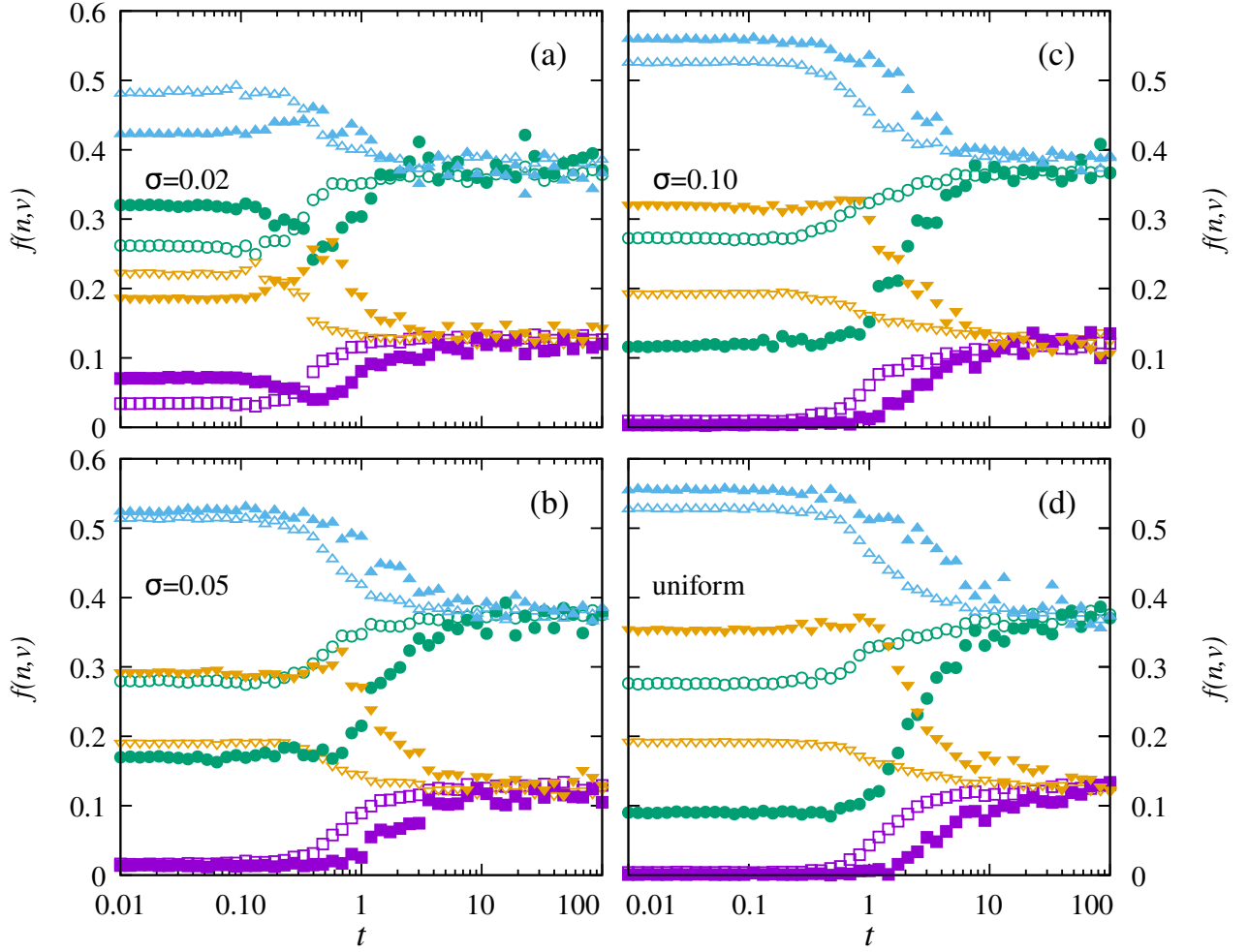


Figure 8: Vertex fraction $f(n, v)$ vs. adimensionalized temperature for different intensity of length fluctuation σ , where $v = 0$: squares (\blacksquare), $v = 1$: circles (\bullet), $v = 2$: up-triangles (\blacktriangle) and $v = 3$: down-triangles (\blacktriangledown), and void points correspond to the fraction of T_1 vertices while filled points to T_3 vertices.

but for this set of parameters it appears only as a shoulder in the vertex population curve, as it overlaps with the second transition into K2 structure, and so, for $d = d_-$ it does not completely develop to 100% of T_1 . In the absence of fluctuations, if $d = d_-$ the K2 arrangement and the ground state (GS) are comprised by T_3 vertices, while if $d = d_+$ they are composed of T_1 vertices. By increasing the intensity of length fluctuations, we have found that the ground state starts to change. For $\sigma = 0.02$, neither the population of T_1 nor T_3 reaches the 100%. For $\sigma \gtrsim 0.05$, low temperature behaviour turns to a 40% T_1 –60% T_3 mixed-state. The error in the final population lowers in comparison to $\sigma = 0.02$, showing more stability. The $P \rightarrow K1$ transition shoulder moves rightward until the transition disappears completely, turning into a $P \rightarrow$ mixed-state transition. This can also be concluded from the examination of the specific heat. Figures 7 (b) and (d) exhibit the corresponding curves, where we show how the $K1 \rightarrow K2$ transition peak disappears when fluctuations are $\sigma \gtrsim 0.02$ and the peak corresponding to $P \rightarrow K1$ transforms into the $P \rightarrow$ mixed-state, displacing rightward and reducing its maximum as the fluctuation intensity increases. In particular, for $d = d_+$ the $K2 \rightarrow GS$ transition peak disappears from the specific heat. To sum up, sufficiently strong length fluctuations removes K1, K2 and the ordered state, replacing them by the 40-60% mixed-state in both $d = d_-$ and $d = d_+$ cases.

Once again, this final state induced by length fluctuation does not correspond to a high temperature random state but to a different behaviour led by asymmetry. We have performed the

same analysis used for square ice, in which we calculated the fraction of vertices $f(n, v)$ with v islands in favour. In Figure 8, we show $f(n, v)$ as a function of temperature t . From the curves, the asymmetry intensified by length fluctuations that appears to explain the difference between T_1 and T_3 population can be seen. Figure 8 (b) shows clearly that at the onset of mixed-state phase, characterized by intensity of length fluctuation $\sigma \approx 0.05$ at low temperatures, the vertex fractions verify the crossover properties $f(1, 1) = f(3, 3)$ and $f(1, 3) = f(3, 1)$, and $f(1, v) = f(3, v)$ for $v = 0, 2$.

4 Conclusions and Perspectives

In summary, we have contributed to the question of how disorder impacts on magnetic frustrated systems by analyzing particularly the effect of nanoislands with design flaws on the thermodynamical properties of the bilayer square and kagome ASI systems. In this work, each island was considered as a dipolar needle and for square ASI the two layers were separated by a distance h . So, as the system's energy depends only on the geometrical parameters of the array, we have proposed selecting each island's length as $d_\kappa = d + \eta_\kappa$, thereby introducing random fluctuations η_κ in the nanoislands' length of the given system according to the probability distribution.

In the square ASI, the mean length d and the parameter h were chosen so that the nearest neighbour J_1 and the next nearest neighbour J_2 interactions were approximately equal. For $h = 0.205a$ and $d = 0.702a$ ($J_1 \lesssim J_2$) or $d = 0.704a$ ($J_1 \gtrsim J_2$), a Gaussian distribution with standard deviation σ has been used up to $\sigma = 0.1$ and then, in order to prevent island overlapping, we have used a uniform distribution between $(-\Delta, \Delta)$. We have established $\sigma \lesssim 0.05$ as the weak disorder range, where the high temperature behaviour remains unchanged, while for low temperature the length fluctuations restore the Ice-like configuration. Furthermore, considering that finding the exact point in the parameter space (d, h_{ice}) where $J_1 = J_2$ is difficult, small flaws turns out to stabilize this state. In contrast, we have shown that strong fluctuations correspond to $\sigma \gtrsim 0.05$. In this regime, we have found that ferromagnetic vertices prevail regardless of whether the mean value of d corresponds to an antiferromagnetic ordering or not. By analyzing the fraction $f(n, v)$ of vertices T_n with v of the four islands favouring them and the energy contained in a T_1 and a T_2 vertex we have found an asymmetry in the system led by strong fluctuations and from which the observed results emerge. Additionally, in the case of uniformly distributed fluctuations, we have found the presence of excitations even in zero temperature.

Complementarily, we have studied the kagome ice inducing a similar situation to that of the square ice system by choosing from the parameter space (J, d) such that it brings $E_1 \approx E_3$. At low temperatures and intensity of length fluctuation above $\sigma \approx 0.05$ the distinctive phases are removed and replaced by a 60% T_1 –40% T_3 mixed ground state. Below, for $\sigma \gtrsim 0.02$, the transition peak $K1 \rightarrow K2$ (gas to ordered phase) disappears and the transition peak $P \rightarrow K1$ (paramagnetic to gas phase) transforms into $P \rightarrow \text{mixed-state}$. In particular, for mean length $d = d_+$ corresponding to energies $E_1 < E_3$, the transition peak $K2 \rightarrow \text{GS}$ (ground state) vanishes. Below $\sigma \approx 0.02$ the four different phases and the transitions between them, described for systems without length fluctuations, are recovered.

Despite being two different systems with a different coordination number, the effect of having flawed islands in the system is similar. In both cases a mixed-state, rather than a random state or an Ice-like state, can be achieved as a result of an intrinsic asymmetry in the dipolar energy which is intensified by the presence of flaws. In kagome ASI, how would the interactions between these two kinds of monopoles be? Could the population of excitations in square ice be increased at zero temperature? It would be interesting to study these issues in the future, taking these results as a starting point.

Acknowledgments

This work was partially supported by Consejo Nacional de Investigaciones Científicas y Técnicas (CONICET), Argentina, PIP 2014/16 N° 112-201301-00629. RCB thanks C Rabini for her suggestions on the final manuscript.

References

- [1] Harris MJ, Bramwell ST, McMorro DF, Zeiske T, Godfrey KW (1997) Geometrical frustration in the ferromagnetic pyrochlore $\text{Ho}_2\text{Ti}_2\text{O}_7$. *Phys Rev Lett* 79: 2554.
- [2] Nisoli C, Moessner R, Schiffer P (2013) *Colloquium*: Artificial spin ice: Designing and imaging magnetic frustration. *Rev Mod Phys* 85: 1473.
- [3] Bramwell ST, Gingras MJP, Holdsworth PCW (2013) Spin ice. In: Diep HT, editor, *Frustrated Spin Systems*, World Publishing Co. 2nd edition.
- [4] Pauling L (1935) The structure and entropy of ice and of other crystals with some randomness of atomic arrangement. *J Am Chem Soc* 57: 2680.
- [5] Ramirez AP, Hayashi A, Cava RJ, Siddharthan RB, Shastry S (1999) Zero-point entropy in ‘spin ice’. *Nature* 399: 333.
- [6] Wang RF, Nisoli C, Freitas RS, J Li WM, Cooley BJ, et al. (2006) Artificial spin ice in a geometrically frustrated lattice of nanoscale ferromagnetic islands. *Nature (London)* 439: 303.
- [7] Bramwell ST, Giblin SR, Calder S, Aldus R, Prabhakaran D, et al. (2009) Measurement of the charge and current of magnetic monopoles in spin ice. *Nature* 461: 956.
- [8] Giblin SR, Bramwell ST, Holdsworth PCW, Prabhakaran D, Terry I (2011) Creation and measurement of long-lived magnetic monopole currents in spin ice. *Nature Phys* 7: 956.
- [9] Mól LA, Silva RL, Silva RC, Pereira AR, Moura-Melo WA, et al. (2009) Magnetic monopole and string excitations in two-dimensional spin ice. *J Appl Phys* 106: 063913.
- [10] Castelnovo C, Moessner R, Sondhi SL (2012) Spin ice, fractionalization, and topological order. *Annu Rev Condens Matter Phys* 3: 35.
- [11] Lieb EH (1967) Residual entropy of square ice. *Phys Rev* 162: 162.
- [12] Möller G (2006) Dynamically reduced spaces in condensed matter physics: Quantum Hall bilayers, dimensional reduction, and magnetic spin systems. Ph.D. thesis, Université Paris Sud - Paris XI. HAL Id: tel-00121765.
- [13] Möller G, Moessner R (2006) Artificial square ice and related dipolar nanoarrays. *Phys Rev Lett* 96: 237202.
- [14] Möller G, Moessner R (2009) Magnetic multipole analysis of kagome and artificial spin-ice dipolar arrays. *Phys Rev B* 80: 140409(R).
- [15] Mól LAS, Pereira AR, Moura-Melo WA (2010) Extending spin ice concepts to another geometry: The artificial triangular spin ice. *Phys Rev B* 85: 184410.
- [16] Nisoli C, Wang R, Li J, McConville WF, Lammert PE, et al. (2007) Artificial square ice and related dipolar nanoarrays. *Phys Rev Lett* 98: 217203.
- [17] Nisoli C, Li J, Ke X, Garand D, Schiffer P, et al. (2010) Effective temperature in an interacting vertex system: Theory and experiment on artificial spin ice. *Phys Rev Lett* 105: 047205.
- [18] Zhang S, Li J, Bartell J, Ke X, Nisoli C, et al. (2011) Ignoring your neighbors: Moment correlations dominated by indirect or distant interactions in an ordered nanomagnet array. *Phys Rev Lett* 107: 117204.

- [19] Rodrigues JH, Mól LAS, Moura-Melo WA, Pereira AR (2013) Efficient demagnetization protocol for the artificial triangular spin ice. *Appl Phys Lett* 103: 092403.
- [20] Arnaluds UB, Farhan A, Chopdekar RV, Kapaklis V, Balan A, et al. (2012) Thermalized ground state of artificial kagome spin ice building blocks. *Appl Phys Lett* 101: 112404.
- [21] Schumann A, Sothmann B, Szary P, Zabel H (2010) Charge ordering of magnetic dipoles in artificial honeycomb patterns. *Appl Phys Lett* 97: 022509.
- [22] Chern GW, Mellado P, Tchernyshyov O (2011) Two-stage ordering of spins in dipolar spin ice on the kagome lattice. *Phys Rev Lett* 106: 207202.
- [23] Tanaka M, Saitoh E, Miyajima H, Yamaoka T, Iye Y (2006) Magnetic interactions in a ferromagnetic honeycomb nanoscale network. *Phys Rev B* 73: 052411.
- [24] Qi Y, Brintlinger T, Cumings J (2008) Direct observation of the ice rule in an artificial kagome spin ice. *Phys Rev B* 77: 094418.
- [25] Zhang S, Gilbert I, Nisoli C, Chern GW, Erickson MJ, et al. (2013) Crystallites of magnetic charges in artificial spin ice. *Nature* 500: 553.
- [26] Li J, Ke X, Zhang S, Garand D, Nisoli C, et al. (2010) Comparing artificial frustrated magnets by tuning the symmetry of nanoscale permalloy arrays. *Phys Rev B* 81: 092406.
- [27] Chern GW, Morrison MJ, Nisoli C (2013) Degeneracy and criticality from emergent frustration in artificial spin ice. *Phys Rev Lett* 111: 177201.
- [28] Chern GW, Mellado P (2016) Magnetic monopole polarons in artificial spin ices. *EPL* 114: 37004.
- [29] Barkema GT, Newman MEJ (1998) Monte Carlo simulation of ice models. *Phys Rev E* 57: 1155.
- [30] Melko RG, Gingras MJP (2004) Monte carlo studies of the dipolar spin ice model. *Journal of Physics: Condensed Matter* 16: R1277.
- [31] Thonig D, Reißaus S, Mertig I, Henk J (2014) Thermal string excitations in artificial spin-ice square dipolar arrays. *Journal of Physics: Condensed Matter* 26: 266006.